Shallow-water vortex equilibria and their stability

2011 J. Phys.: Conf. Ser. 318 062019

(http://iopscience.iop.org/1742-6596/318/6/062019)

Journal of Physics: Conference Series **318** (2011) 062019 doi:10.1088/1742-6596/318/6/062019

Shallow-water vortex equilibria and their stability

H Płotka and D G Dritschel

School of Mathematics and Statistics, University of St Andrews, North Haugh, St. Andrews KY16 9SS, UK

E-mail: hanna@mcs.st-andrews.ac.uk, dgd@mcs.st-andrews.ac.uk

Abstract. We first describe the equilibrium form and stability of steadily-rotating simply-connected vortex patches in the single-layer quasi-geostrophic model of geophysical fluid dynamics. This model, valid for rotating shallow-water flow in the limit of small Rossby and Froude numbers, has an intrinsic length scale L_D called the 'Rossby deformation length' relating the strength of stratification to that of the background rotation rate. Specifically, $L_D = c/f$ where $c = \sqrt{gH}$ is a characteristic gravity-wave speed, g is gravity (or 'reduced' gravity in a two-layer context where one layer is infinitely deep), H is the mean active layer depth, and f is the Coriolis frequency (here constant). We next introduce ageostrophic effects by using the full shallow-water model to generate what we call 'quasi-equilibria'. These equilibria are not strictly steady, but radiate such weak gravity waves that they are steady for all practical purposes. Through an artificial ramping procedure, we ramp up the potential vorticity anomaly of the fluid particles in our quasi-geostrophic equilibria to obtain shallow-water quasi-equilibria at finite Rossby number. We show a few examples of these states in this paper.

1. Introduction

Vortices are self-organized fluid dynamical structures which spontaneously arise in turbulent flows (see for example (McWilliams, 1984)). They are of great importance in geophysical fluid dynamics, and are an omnipresent feature of the Earth's oceans and atmosphere, as well as the atmospheres of the giant gas planets. Ebbesmeyer *et al.* (1986) estimates that there are over 10,000 vortices in the surface layers of the North Atlantic alone, and examples of terrestrial atmospheric vortices include such long-lived features as mid-latitude cyclones and the 'polar vortex', which dominates the extratropical winter stratosphere (Norton, 1994).

Vortices may be regarded as 'balanced' flow features, whose velocity and thermodynamical fields are largely self-induced, essentially by their distribution of 'potential vorticity'. Geophysical flows may meaningfully be split into two components: (1) a dominant, long-lived (compared to a characteristic time such as a day) balanced component consisting of vortices, fronts and jets, and (2) a weaker, higher-frequency, relatively disorganised unbalanced component consisting of inertia-gravity waves.

Turbulent geophysical flows are hugely complicated. As a first step towards understanding them, therefore, it may be useful to examine them through this concept of balance. A tool to do this is the quasi-geostrophic (QG) approximation, which filters out the unbalanced, gravity-wave component, and retains only the balanced, vortical motions.

In this study, we use the QG model as a starting point to investigate the forms of vortex equilibria and their stability, which to date have not been fully documented even for the

simplest case of a single vortex patch consisting of uniform potential vorticity (PV). In 1893, Love examined the 'barotropic' (or 2D Euler) case of an elliptical vortex patch, and showed analytically that all vortices having an aspect ratio $\lambda \geq 1/3$ are linearly stable, while those having $\lambda < 1/3$ are unstable (Love, 1893). Nearly a century later, this was confirmed numerically, for finite-amplitude disturbances (Dritschel, 1986). Nearly all studies to date have considered only the barotropic model, applicable only when the Rossby deformation radius L_D is infinite. The few exceptional studies include Polvani *et al.* (1989) and Flierl (1988). Here, we fully document the steadily-rotating equilibria together with their linear and nonlinear stability for a single vortex patch. In the QG model, such equilibria are spanned by two parameters, L_D and λ.

This study then goes further to examine vortex 'quasi-equilibria' in the parent shallow-water equations, a model which does permit gravity waves. Using a novel ramping procedure within the full equations of motion, we are able to generate approximate equilibria (unsteady only due to extremely weak gravity wave radiation), and at the same time investigate their (nonlinear) stability. That is, at some critical amplitude of the PV inside the vortex (related to the Rossby number), the vortex exhibits a rapid change in shape, often splitting into two or more parts.

2. Quasi-geostrophic equilibria

We first use the quasi-geostrophic shallow-water (QGSW) model to generate steady states. Despite its great simplicity (it is two-dimensional and does not allow gravity waves), it is perhaps the most popular model for the study of the fundamental aspects of atmospheric and oceanic (geophysical) flows (Vallis, 2008). We use the simplest form of the model, with no forcing, no damping, no topography and constant planetary vorticity f. We use the 1-1/2 layer model, in which we have a two layer system with a rigid lid and bottom. We take the lower layer to be infinitely deep. The QG model consists of a single 'prognostic' equation for the material (conservative) advection of QG potential vorticity q,

$$\frac{\mathrm{D}q}{\mathrm{D}t} = \frac{\partial q}{\partial t} + u\frac{\partial q}{\partial x} + v\frac{\partial q}{\partial y} = 0, \tag{1}$$

and a Helmholtz-type 'inversion relation' providing the (non-divergent) flow field $\boldsymbol{u}$ from q,

$$(\nabla^2 - L_D^{-2})\psi = q \quad ; \quad u = -\frac{\partial \psi}{\partial y} \quad ; \quad v = \frac{\partial \psi}{\partial x}, \tag{2}$$

where $L_D = c/f$ is the Rossby deformation length. The importance of L_D is that fluid motions at scales $L \ll L_D$ behave in the classical two-dimensional (2D) manner, with negligible free-surface deformation (as in the 2D Euler equations), whereas motions at scales $L \gg L_D$ are strongly affected by these deformations.

We thus generate vortex patches of uniform QG PV $q = q_0$ (with $q = 0$ outside the vortex). They are entirely prescribed by the vortex's boundary shape, and we seek shapes which are preserved under dynamical evolution – these are often referred to as 'relative equilibria', but here we simply call them equilibria. We seek two-fold symmetric simply-connected shapes, and work in terms of $\gamma = L/L_D$.

A few examples of the vortex shapes are shown in figure 1. Except in the limiting barotropic case, they deform into dumbbell shapes as their aspect ratio λ is reduced. Their linear stability is summarised in figure 2, which shows contour plots of the two primary growth rates as a function of the aspect ratio λ and inverse Rossby deformation radius γ. Love's barotropic results are obtained in the limit $\gamma \to 0$.

Further details about the properties and stability of such vortices may be found in Płotka & Dritschel (2011).

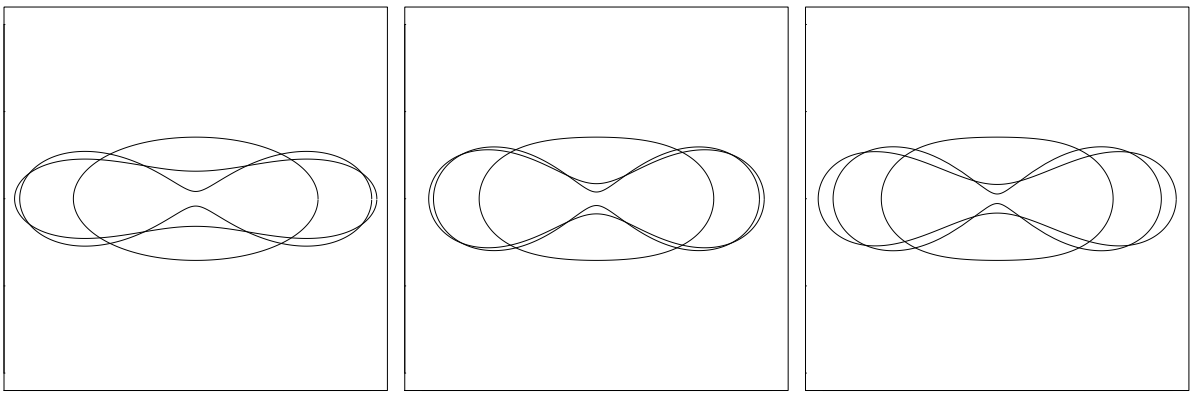

Figure 1. Selected equilibrium contour shapes for $\gamma = 0.5$ (left), 3.0 (middle), and 8.0 (right). In each frame, we show the equilibrium contours for $\lambda = 0.5$, for the largest stable aspect ratio λ_c, and for the smallest aspect ratio attainable λ_f. The plot window is the square $|x|, |y| \leq 2.2$.

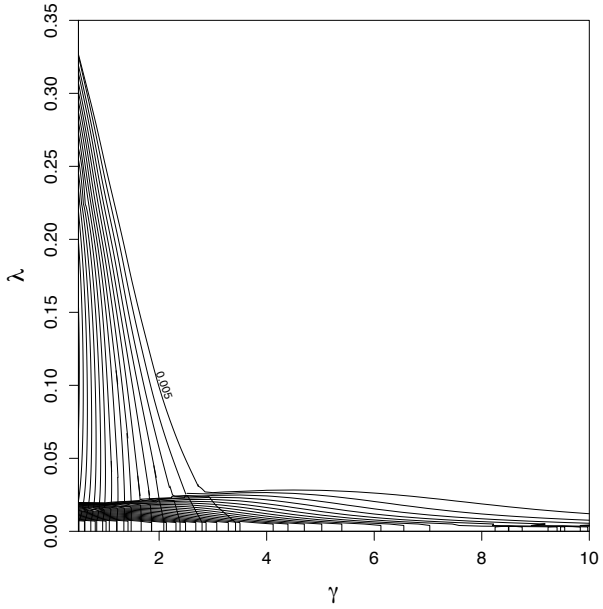

Figure 2. Growth rates σ_r of modes 1 and 2 in the γ-λ parameter plane. 30 contour levels are shown, and the contour interval is 0.005.

3. Shallow-water equilibria

We next use the full shallow-water model (which permits gravity waves) to introduce ageostrophic effects in our model. The full shallow-water equations we solve are:

$$\frac{Du}{Dt} - fv = -c^2 \frac{\partial h}{\partial x} \tag{3}$$

$$\frac{Dv}{Dt} + fu = -c^2 \frac{\partial h}{\partial y} \tag{4}$$

$$\frac{\partial h}{\partial t} + \nabla \cdot (\boldsymbol{u} h) = 0 \tag{5}$$

where $\boldsymbol{u} = (u(x, y, t), v(x, y, t))$ is the (horizontal) velocity, f is the Coriolis parameter (twice the background rotation rate Ω), $h(x, y, t)$ is the fluid depth (or height) scaled on the mean fluid depth H, and $c = \sqrt{gH}$ is the short-scale mean gravity wave speed.

We solve the by using the contour advective semi-Lagrangian (CASL) algorithm, in which we keep track of contours of constant potential vorticity, and of velocity and pressure on a grid (Dritschel & Ambaum, 1997; Smith & Dritschel, 2006).

We generate what we call 'quasi-equilibria' by using the QG equilibria described above. Our new equilibria are not strictly steady, but radiate such weak gravity waves that they are steady for all practical purposes. Starting with a QG equilibrium (having zero Rossby number $\mathcal{R}$), we perform an artificial ramping procedure called 'dynamic PV initialisation' (Viúdez & Dritschel, 2004). In this procedure, the shallow-water PV anomaly on every fluid particle is ramped up to a final value while integrating the full equations of motion. This is artificial because the PV anomaly is conserved on fluid particles. However, at the end of the ramping period, the PV is thereafter conserved, and the flow obtained tends to have exceedingly weak gravity wave activity, especially if a long ramp period is considered. In this way, we generate many quasi-equilibria at finite Rossby number.

The long-time, in many cases, persistence of the quasi-equilibria testifies to their stability. We further examine their steadiness by looking at the extent to which the contours of the Bernoulli function coincide with those of the PV. For rotating shallow-water flows, the Bernoulli function takes the form

$$p = hc^2 + \frac{1}{2}|\boldsymbol{u}_{rot}|^2 - \frac{1}{2}\Omega f(x^2+y^2) \tag{6}$$

with $\boldsymbol{u}_{rot} = (u + \Omega y, v - \Omega x)$ and Ω the rotation rate. This is true for an appropriately-chosen rotating frame of reference.

The steadiness parameter, ϵ_b, is a dimensionless measure defined as

$$\epsilon_b = \frac{\sqrt{\frac{1}{L}\oint_C (p-\bar{p})^2 dS}}{\bar{p}} \tag{7}$$

where $L = \oint_C dS$ is the arc length of the PV contour, and $\bar{p} = (1/L)\oint_C p dS$ is the mean Bernoulli pressure around the PV contour. ϵ_b measures the r.m.s. of the difference between p and $\bar{p}$ around a constant PV contour, normalised by $\bar{p}$. Values close to zero indicate that that constant Bernoulli and PV contours coincide, and non-zero values point towards the state being unsteady.

Several examples of the quasi-equilibria generated, and their values of ϵ_b are shown in the following section.

4. Several examples of quasi-equilibria

Here we show three examples of the quasi-equilibria we generate. We first show a stable steady state, and then show two types of instabilities found.

4.1. Example 1: Steady quasi-equilibrium

The first example we show is that of a steady state in figure 4. We chose to look at $\gamma = 10$, Rossby number $\mathcal{R} = -0.01$ at aspect ratio $\lambda = \lambda_c = 0.025$ (this corresponds to the last stable equilibrium in the QG model). The ramping period lasts until $t = 20$ (in this and subsequent examples), after which the state is allowed to evolve freely for a comparable time. We see a very close correspondence between the Bernoulli function and PV contours, and as time passes, we have no change in shape of the vortex. The steepest growth of the Bernoulli function occurs around the vortex boundary – here we have a change of p measuring 0.003, whereas the change between the edge of the vortex and the domain boundary is just 0.001. This is typical of steady states having large γ values. When we examine the steadiness parameter ϵ_b in the left-most plot of figure 3, we see that both during and after the ramp period we have a constant, low

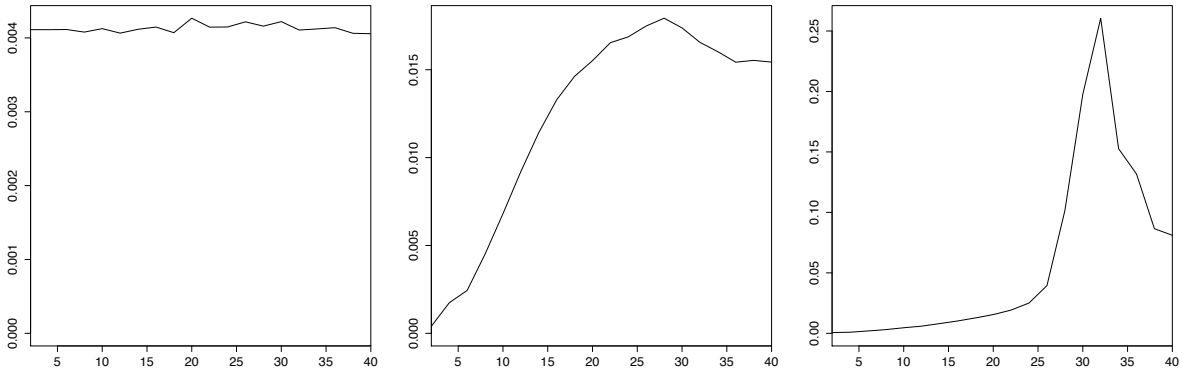

Figure 3. Values of the steadiness parameter ϵ_b through time for $\gamma = 10$, $\mathcal{R} = -0.01$, $\lambda = 0.025$ (left), $\gamma = 3$, $\mathcal{R} = 0.5$, $\lambda = 0.031$ (middle), and $\gamma = 3$, $\mathcal{R} = -0.3$, $\lambda = 0.031$ (right).

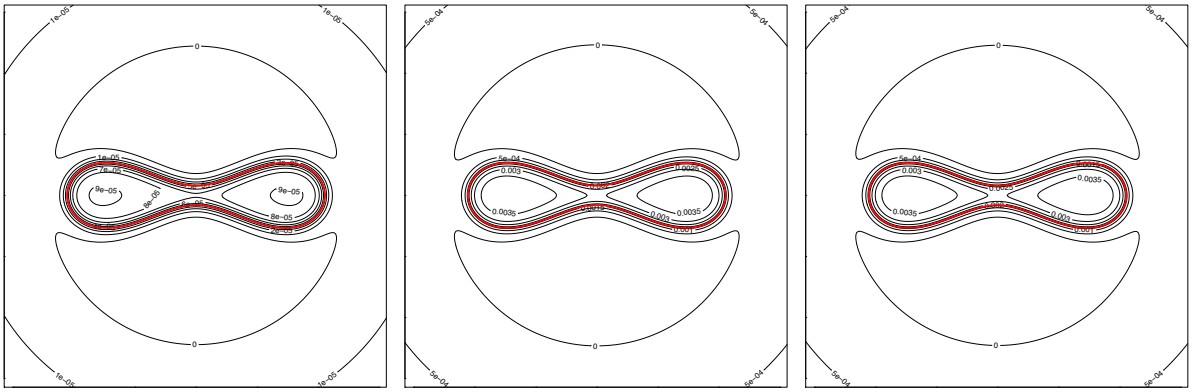

Figure 4. The potential vorticity contour (red) and Bernoulli function contours (black) for $\gamma = 10$, $\mathcal{R} = -0.01$, $\lambda = 0.025$ at times $t = 1$ (left), $t = 20$ (middle), and $t = 40$ (right). Here, $|x|, |y| \leq \pi$.

value, which indicates that the state remains steady for all time. Ramping PV does not seem to greatly influence stability, which is expected as here we do not ramp the PV to a very high value.

4.2. Example 2: Unstable quasi-equilibrium, deformation

The second example shows an unstable quasi-equilibrium, having $\gamma = 3$, Rossby number $\mathcal{R} = 0.5$, and aspect ratio $\lambda = \lambda_c = 0.031$. In figure 5 we once again see that the Bernoulli function and PV contours coincide quite closely for all time. However, unlike in example 1, we now have a deformation in the shape of the quasi-equilibrium. The aspect ratio increases, as time progresses, and the equilibrium becomes more elliptical rather than dumbbell-shaped. We also note that the change in the Bernoulli function is more gradual across the domain, and is not limited to only around the vortex boundary. By looking at ϵ_b in middle plot of figure 3, we see that the values are much higher than for the stable case (note the different vertical scales). We see a gradual increase until time $t = 20$ during the ramp period. ϵ_b then continues to increase, roughly until $t = 28$, after which it decreases slightly. This would seem to indicate that the vortex is re-adjusting itself to tend to some new quasi-equilibrium. The larger ϵ_b during the ramp period is also and indication of the fact that we now have much higher values of the Rossby number than previously.

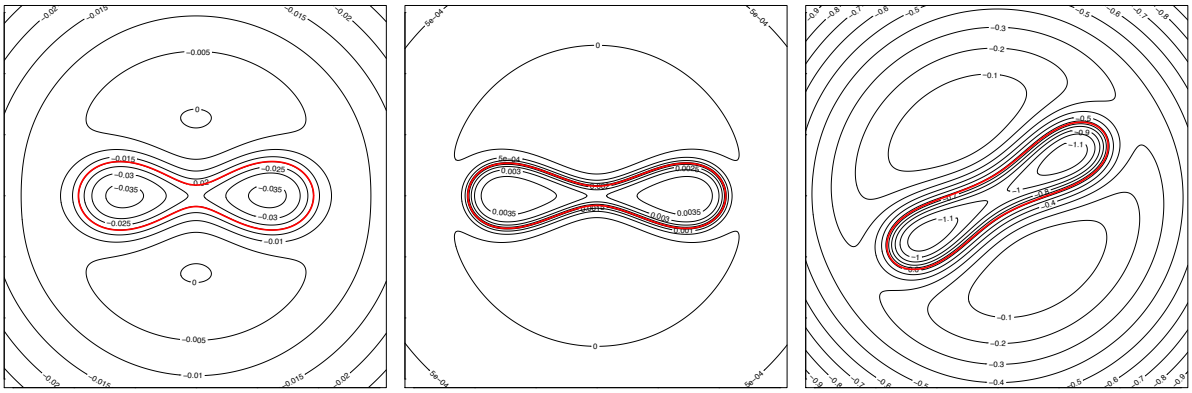

Figure 5. The potential vorticity contour (red) and Bernoulli function contours (black) for $\gamma = 3$, $\mathcal{R} = 0.5$, $\lambda = 0.031$ at times $t = 1$ (left), $t = 20$ (middle), and $t = 40$ (right). Here, $|x|, |y| \leq \pi$.

4.3. Example 3: Unstable quasi-equilibrium, split

The final example shows the $\gamma = 3$, Rossby number $\mathcal{R} = -0.3$ at $\lambda = \lambda_c = 0.031$ case. Here we see the quasi-equilibrium splitting into two. By looking at figure 6, we see that we have a very quick split, with the Bernoulli contours corresponding to the PV contours very closely both before and after the split. Indeed, when we look at ϵ_b in the right-most plot of figure 3, we see that we get a sudden spike at roughly time $t = 32$, after which it falls back down significantly. This corresponds to the time at which the vortex has already split into two, and is trying to re-align itself with the Bernoulli contours to regain some sort of stability. In this case, the values of ϵ_b are much higher than for the previous two cases – the change in shape of the vortex is most drastic.

5. Outlook

We have here presented a few examples of shallow-water quasi-equilibria, and have performed a first step into assessing their stability. We have found different sorts of behaviour occurring, including a split and shape deformation of the vortex, depending on initial conditions. Future work includes expanding the parameter space, and examining the behaviour of these quasi-equilibria over a wider range of aspect ratios, Rossby deformation lengths and Rossby numbers.

References

Dritschel, D G 1986 The nonlinear evolution of rotating configurations of uniform vorticity. *J. Fluid Mech.* **172**, 157–182.

Dritschel, D G & Ambaum, M H P 1997 A contour-advective semi-lagrangian algorithm for the simulation of fine-scale conservative dynamical fields. *Quart. J. Roy. Meteorol. Soc.* **123**, 1097–1130.

Ebbesmeyer, C C, Taft, B A, McWilliams, J C, Shen, C Y, Riser, S C, Rossby, H T, Biscaye, P E & Östlund, H G 1986 Detection, structure, and origin of extreme anomalies in a Western Atlantic oceanographic section. *J. Phys. Oceanogr.* **16**, 591–612.

Flierl, G R 1988 On the instability of geostrophic vortices. *J. Fluid Mech.* **197**, 349–388.

Love, A E H 1893 On the stability of certain vortex motions. *Proc. London Math. Soc.* **25**, 18–42.

McWilliams, J C 1984 The emergence of isolated coherent vortices in turbulent flow. *J. Fluid Mech.* **146**, 21–43.

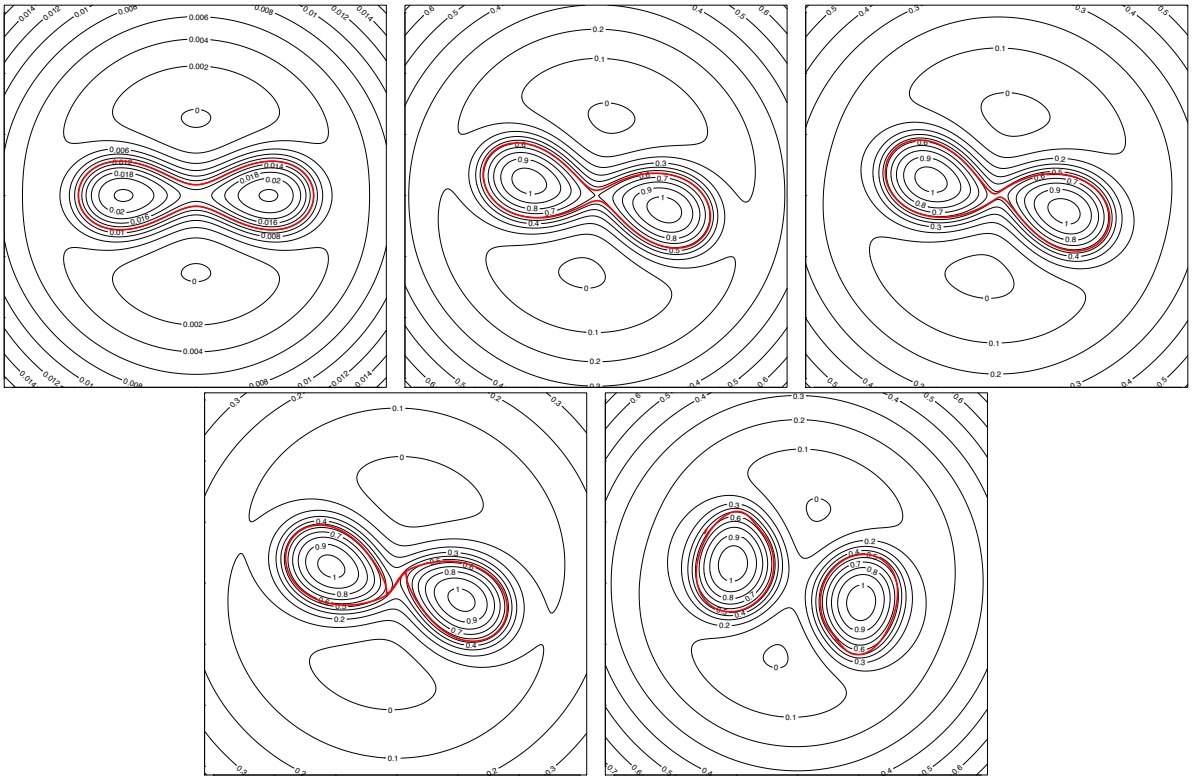

Figure 6. The potential vorticity contour (red) and Bernoulli function contours (black) for $\gamma = 3$, $\mathcal{R} = -0.3$, $\lambda = 0.031$ at times $t = 1$ (upper left), $t = 24$ (upper middle), $t = 26$ (upper right), $t = 28$ (lower left), and $t = 40$ (lower right). Here, $|x|, |y| \leq \pi$.

Norton, W A 1994 Breaking Rossby waves in a model stratosphere diagnosed by a vortex-following coordinate system and a technique for advecting material contours. *J. Atmos. Sci.* **51**, 654–673.

Płotka, H & Dritschel, D G 2011 Quasi-geostrophic shallow-water vortex-patch equilibria and their stability. *In preparation* .

Polvani, L M, Zabusky, N J & Flierl, G R 1989 Two-layer geostrophic vortex dynamics. part 1. upper-layer v-states and merger. *J. Fluid Mech.* **205**, 215–242.

Smith, R & Dritschel, D G 2006 Revisiting the rossby-haurwitz wave test with contour advection. *J. Comput. Phys.* **217**, 473–484.

Vallis, G K 2008 *Atmospheric and Oceanic Fluid Dynamics*. Cambridge University Press.

Viúdez, Á & Dritschel, D G 2004 Dynamic potential vorticity initialization and the diagnosis of mesoscale motion. *J. Phys. Oceanogr.* **34**.